PCCP

PAPER

View Article Online
View Journal | View Issue

Cite this: *Phys. Chem. Chem. Phys.*, 2016, **18**, 4527

Anisotropic kinetics of solid phase transition from first principles: alpha–omega phase transformation of Zr†

Shu-Hui Guan and Zhi-Pan Liu*

Structural inhomogeneity is ubiquitous in solid crystals and plays critical roles in phase nucleation and propagation. Here, we develop a heterogeneous solid–solid phase transition theory for predicting the prevailing heterophase junctions, the metastable states governing microstructure evolution in solids. Using this theory and first-principles pathway sampling simulation, we determine two types of heterophase junctions pertaining to metal α–ω phase transition at different pressures and predict the reversibility of transformation only at low pressures, *i.e.* below 7 GPa. The low-pressure transformation is dominated by displacive Martensitic mechanism, while the high-pressure one is controlled by the reconstructive mechanism. The mechanism of α–ω phase transition is thus highly pressure-sensitive, for which the traditional homogeneous model fails to explain the experimental observations. The results provide the first atomic-level evidence on the coexistence of two different solid phase transition mechanisms in one system.

Received 26th November 2015,
Accepted 4th January 2016

DOI: 10.1039/c5cp07299a

www.rsc.org/pccp

1. Introduction

Heterogeneity is intrinsic to solid–solid phase transition, being the key feature in nucleation and anisotropic phase propagation.[1,2] The nature and behavior of anisotropic transition intermediates represent a critical area in the development of a basic understanding of the evolution of microstructures during processing and heat treatment of materials. However, the heterogeneous kinetics constantly challenges traditional theory in the homogeneous, phenomenological framework.[3,4] Specifically, the energy profile of solid phase transition, unlike molecular reactions, is extremely difficult to establish for the lack of tools to resolve the unknown interphase interfaces in phase growth, the structure of which is related to the collective atom displacement in phase transition. This has given us poor understanding on many basic facts even in prototypical solid systems,[5] *e.g.* the nature of nuclei, the structure of heterophase junctions, the phase growth pattern, and the crystallographic orientation relationship (OR). Here, using kinetics theory and first-principles simulation based on novel potential energy surface sampling techniques, we propose a heterogeneous model for computing and predicting the anisotropic kinetics in diffusionless solid phase transition. This is demonstrated in the α–ω phase transformation of the Group IV metal Zr, where our theory rationalizes the contradictory OR and reversibility from various experiments in the past 50 years.

Group IV metals (Ti, Zr) and their alloys are known as lightweight, high-strength and oxidation-resistant materials in many industrial applications.[5–8] They have three common phases: the hexagonal close-packed α phase ($P6_3/MMC$, no. 194), most stable at ambient condition; the simple hexagonal ω phase ($P6/mmm$, no. 191) at higher pressure (~5 GPa); and the body-centered-cubic β phase ($Im\bar{3}m$, no. 229) at high temperature (>1100 K) and high pressure (>30 GPa).[5,9–13] For their apparently simple crystal structure, the transition between different phases is extensively studied as the model systems of solid phase transition. The α-to-ω phase transition occurring typically above ~2 GPa, in particular, significantly increases the brittleness of the material, and thus is of practical importance for applications of the material under extreme conditions.[14,15] However, due to the lack of microscopic information on the transition pathways, the α–ω phase transition, although studied extensively, remains a highly challenging system for experiment and theory, where many basic facts of phase kinetics are highly controversial, including the ORs, the nature of intermediate, and the pressure and temperature dependence.

The α-to-ω phase transition has long been known as a diffusionless solid phase transition due to the observation of OR between α and ω phase in experiment using X-ray diffraction and transmission electron microscopy. However, static pressure and shock-loaded experiments[16–27] have observed two different

Collaborative Innovation Center of Chemistry for Energy Material, Key Laboratory of Computational Physical Science (Ministry of Education), Shanghai Key Laboratory of Molecular Catalysis and Innovative Materials, Department of Chemistry, Fudan University, Shanghai 200433, China. E-mail: zpliu@fudan.edu.cn

† Electronic supplementary information (ESI) available. See DOI: 10.1039/c5cp07299a

crystallographic ORs, namely, Variant-I: $(0001)_\alpha//(01\bar{1}1)_\omega$; $[11\bar{2}0]_\alpha//[10\bar{1}1]_\omega$ and Variant-II: $(0001)_\alpha//(11\bar{2}0)_\omega$; $[11\bar{2}0]_\alpha//[0001]_\omega$, implying at least two different pathways occurring in α–ω phase transition. This fact is unusual considering that the minimum number of atoms per unit cell in transition is only six. These two ORs were initially suggested by Usikov and Zilbershtei (UZ)[16] by considering β phase as an intermediate in phase transition. Interestingly, only Variant-I OR was in fact observed in UZ experiment. Later experiments on Zr metal did not observe the intermediate β phase[17,18] and generally identify only one type of OR, either Variant-I or Variant-II, depending on experimental setups (see ESI,† for an overview), for example, Variant-I from Song *et al.*[18] and Jyoti *et al.*,[19] and Variant-II from Rabinkin *et al.*,[17] Kustar *et al.*[22] and Wenk *et al.*[23]

A further complication is the reversibility of the transformation with and without pressure loading, where both perfect reversibility and significant dislocation/defect creation were reported in different experiments (*e.g.*, ref. 23 and 28). Both isothermal and athermal phase transition kinetics behaviors were observed at different static and dynamic pressure conditions.[5,14,27] These experimental facts on the pressure and temperature dependence kinetics also suggest complex reaction kinetics that may vary the mechanism under different experimental conditions.

However, recent theoretical results in the homogeneous framework are at odds with the experimental findings. Based on the lattice and atom correspondence of ORs, theoretical calculations[29,30] established the homogeneous phase transition pathways (*i.e.* α → ω transition without passing intermediate α/ω heterophase junction). It was found that the pathway with Variant-I OR has much lower barrier than that with Variant-II, which suggests only Variant-I is likely under experimental conditions. This challenges the observation of Variant-II OR and the dependence of kinetics on experiment conditions (*e.g.* the pressure).

The puzzle of the metal α–ω phase transformation reflects the current difficulties of using the homogeneous theory for treating the crystal phase transition, which totally neglects the critical role of phase transition intermediates. This is partly because it is difficult, using a traditional approach such as molecular dynamics, to capture the transition events and to resolve the heterogeneity in the transition process in the presence of the high reaction barrier in solid phase transition. The quantum mechanics treatment of solid phase transition is thus largely limited in the homogeneous transformation model, where the OR and the pathway are pre-guessed or configured according to the experimental data. While the heterogeneous model is desirable, there are still many difficulties in simulation, including finding reaction pathways and identifying the structure of reaction intermediates, such as the heterogeneous phase junctions.

2. Theory for heterogeneous phase transition

In this work, we start by proposing a heterogeneous phase transition model, which is applied to establish the anisotropic phase transition pathway. We show that the automated PES sampling method developed recently can be fitted into this model by providing the critical information on the atom displacement patterns, from which the anisotropic pathways and the interphase interfaces can be resolved at the atomic level.

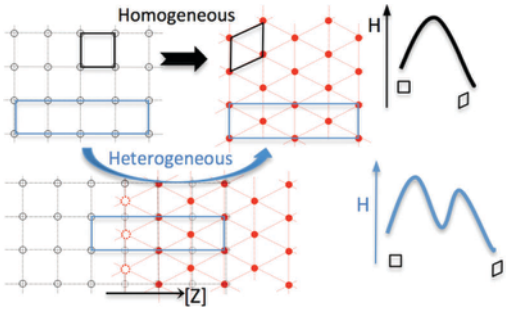

Fig. 1 Illustration of the homogenous (black) and heterogeneous (blue) phase transition models in 2D lattice (square-to-hexagonal transition) together with their schematic energy profiles. Each heterogeneous pathway is along a crystallographic direction [*Z*] *via* the corresponding heterophase junction (*e.g.* with square/hexagonal interface). The lowest barrier pathway should dominate the kinetics, dictating the phase propagation direction.

Fig. 1 illustrates our main idea on the heterogeneous phase transition model, comparing it with the traditional homogeneous phase transition model. The homogeneous model displaces all atoms simultaneously from one phase to another, neglecting the likely metastable intermediates and lacking the kinetics information on the prevailing phase propagation directions. The enthalpy ($H = E + PV$) barrier of solid phase transition is measured on the basis of per bulk atom.

In contrast, the heterogeneous model incorporates the metastable intermediates in the pathway. Because these intermediates are naturally crystallographic direction-dependent, the energy profile will reflect the anisotropic behavior of kinetics. Generally, the behavior of the transformation front ultimately governs the resultant morphology of the products and, therefore, the resultant physical and mechanical properties of the material. The challenge is then to identify the metastable states that are vital to the lowest energy channels of transition. For diffusionless solid phase transition, the preferable intermediates are associated with the heterophase junctions (HJ) with low strain, coherent interfaces, as illustrated in Fig. 1. By determining these HJs and the energy profile, one can derive the heterogeneous enthalpy barrier $H_a[Z]$ and thus kinetics at a given crystallographic direction [*Z*].

In the following, we demonstrate the theory using the α–ω phase transition of Zr. We show that the energy profile of heterogeneous phase transition pathways can be established rigorously from first principles *via* a four-step procedure, where the state-of-the-art crystal pathway sampling acts as the key tool to identify all likely atom displacement patterns.

3. Methodology and calculation methods

3.1 Stochastic surface walking (SSW) pathway sampling

The SSW methodology has been described in our previous work in detail.[31,32] We have shown that the SSW method is able to

explore the potential energy surface (PES) to identify unexpected new structures, including clusters and crystals, and in the meantime collect the reaction pathways leading to them. The purpose of SSW crystal pathway sampling is to establish a one-to-one correspondence for lattice (L($\boldsymbol{e}_1$,$\boldsymbol{e}_2$,$\boldsymbol{e}_3$), $\boldsymbol{e}_i$ being the lattice vector) and atom (q_i, i = 1,...3N; N is the number of atoms in cell) from one phase to another. The lattice here is not necessarily the conventional lattice, but any possible lattice set that describes the same crystal phase. Using such a pair of coordinates, Q_{IS}(L, q) and Q_{FS}(L, q) (IS and FS are the initial and the final states), it is then possible to utilize a double-ended transition state searching method to identify the reaction pathway and the transition state. The procedure of SSW pathway sampling is briefly described below.

Pathway collection. Firstly, we start from one single phase (starting phase) and utilize the SSW method to explore all the likely phases near that phase. A structure selection module is utilized to decide whether to accept/refuse a phase once a new minimum is reached. If the new phase that is different from the starting phase is identified by the SSW crystal method,[33] we record/output the IS (*i.e.* starting phase) and the FS (a new phase) of the current SSW step. Then, the program returns to the IS by rejecting the new minimum to continue the phase exploration. On the other hand, if the new minimum identified by SSW is still the starting phase (*e.g.* the same symmetry, but a permutation isomer with varied lattice), the program will accept the new isomeric phase and start the phase exploration from this phase. We repeat this procedure until a certain number of IS/FS pairs are reached.

Pathway screening. Secondly, we utilize the variable-cell, double-ended surface walking (DESW) method[34] to establish the pseudopathway connecting IS to FS for all IS/FS pairs.[35,36] The approximate barrier is obtained according to DESW pseudo-pathway, where the maximum energy point along the pathway is generally a good estimate for the true TS.[34] By sorting the approximate barrier height, we can obtain candidates for the lowest energy pathways. At this stage, we have generally thoroughly examined all the pathways we identified. Even before we exactly locate the TS, we have the following important information, including the approximate barrier, the pattern of lattice and atom movement from IS to FS, the atomic habit plane and the OR for the pathways. From these, we can safely rule out similar pathways and focus on the selected, distinct and low-energy pathways.

Lowest-energy pathway determination. Thirdly, the candidate lowest energy pathways are selected to locate exactly the "true" TS by using the DESW TS-search method for crystal systems.[34,37] The performance of DESW method for finding the TS of solid phase transition has been benchmarked with the generalized solid-state nudged-elastic-band (G-SSNEB) method[38] in our recent work.[37] By sorting the exact barrier calculated, the energy difference between the TS and the IS, the lowest energy pathways, can be finally obtained. All the lowest energy pathways are further confirmed by extrapolating TS towards IS and FS, and the TSs are validated by phonon spectrum calculation, showing one and only one imaginary mode.

3.2 Density functional theory (DFT) calculations

All calculations were performed using the plane wave DFT program, Vienna ab initio simulation package VASP[39,40] where the Zr electron–ion interaction was represented by the projector-augmented wave (PAW),[41] and the exchange–correlation functional utilized was GGA-PBE.[42] In the pathway sampling, we adopt the following setups to speed up the PES exploration: plane-wave cutoff, 400 eV; the Monkhorst–Pack k-point ($6 \times 6 \times 6$) mesh set for the 6-atom supercell and the ($4 \times 4 \times 4$) set for the 12-atom supercell; and 4-electron (4d5s) PAW pseudopotential for Zr. To obtain accurate energetics for the pathways, a more accurate calculation setup was utilized: the plane-wave cutoff, 600 eV; the k-point mesh up to ($10 \times 10 \times 10$) set; and 12-electron (4s4p4d5s) PAW pseudopotential for Zr. For all the structures, both lattice and atomic positions were fully optimized until the maximal stress component was below 0.1 GPa and the maximal force component below 0.001 eV Å^{-1}, which leads to the convergence of the relative energy (*e.g.* barrier) below 2 meV per atom. The convergence of the energetics with respect to k-point mesh is shown in Table SII (ESI†). The phonon frequencies of the crystals were determined using the finite displacement method,[43, 44] which is utilized to confirm the obtained TS with one and only one imaginary frequency across the first Brillouin zone.

4. Results and discussion

4.1 Mechanism and anisotropic pathways

To understand the overall mechanism of solid phase transition, it is essential to determine a set of anisotropic pathways as required by the heterogeneous phase transition model in Fig. 1. Obviously, this is the most challenging part in the heterogeneous phase transition model. It is in principle possible to directly utilize the automated PES sampling techniques such as SSW to sample the anisotropic pathways in large supercells of the crystal, where the heterophase junctions are born naturally in the lowest energy pathway. However, such simulations are practically unfeasible for the high computational demand in the first-principles framework, considering that thousands of pathways need to be sampled in order to reveal the lowest-energy one.

In this work, we adopt an indirect approach to identify the lowest-energy anisotropic pathway. This approach is described as follows. First, the automated PES sampling is utilized only for homogeneous pathway sampling, which produces atom displacement patterns in the phase transition. Multiple low-energy homogeneous pathways are considered as possible patterns (*e.g.* OR) related to heterogeneous phase propagation. This is unlike the treatment in the traditional homogeneous model that usually focuses only on the lowest energy one. Next, using the atom displacement patterns, we then construct the anisotropic phase transition pathway using a superlattice approach and finally reveal the anisotropic phase propagation pathways. The detailed procedure includes four steps, which are elaborated in the following.

a. Crystal pathway sampling and homogenous pathways. First, we utilize DFT-based SSW for crystal method to sample the phase space of Zr metal at 3 GPa, unbiasedly and exhaustively. We have collected 263 α–ω phase transition pathways represented by a database of initial and final state pairs (IS/FS), which is gleaned from SSW potential energy surface exploration of 5777 minima in the 6-atom cell and 2193 minima in the 12-atom cell (note that the large cell pathway sampling is computationally much more demanding, and thus, less minima are collected in practice). From these minima, we can identify all the common phases, including the simple hexagonal phase (ω, the global minimum at 3 GPa), the α phase, the body-center cubic (bcc, no. 229), and the other possible phases, such as face-center cubic (fcc, no. 225) and a cubic phase (no. 139), as well as the less ordered structures, as shown in Fig. 2a. This reflects that SSW sampling is able to explore the PES of Zr in a large area and therefore can in principle capture the allowed homogeneous phase transition pathways.

$$C = \frac{C_0}{N_0}\sum_{i=1}^{N_0}\sum_{j=1(i\neq j)}^{N}\frac{1}{1+e^{d_{ij}-d_0}} \quad (1)$$

To show an overview of these different phases, we have plotted in Fig. 2b the volume of the phase against the coordination of Zr. The figure reflects the structure features of these common phases. The metal coordination C is defined as eqn (1) to maximally distinguish the common phases. In eqn (1), N_0 is the number of Zr atoms in the primitive cell, and N is the number of Zr atoms in the supercell ($(3 \times 3 \times 3)$ of the primitive cell); i and j are the atom labels; d_{ij} is the distance between the i atom and j atom; d_0 is a constant equal to 3.24 (Å); C_0 is a scaling constant equal to 1.33, to yield ~12-coordination for Zr in α phase.

Fig. 2b shows that α and ω phases are the two most stable phases at the 3 GPa condition, which differ largely in the volume and the coordination (well separated in the figure). On the other hand, the less stable phases, β and fcc phases, are structurally closer to α and ω phases with similar volume and coordination. Indeed, UZ first proposed that the α–ω phase transition bypasses the β phase intermediate based on the structural similarity. The β-phase–mediated mechanism can explain the two types of OR observed in different experiments. However, this mechanism remains highly controversial because β phase is less stable, and thus the pathway *via* β phase must have a high barrier. β phase was not observed in the subsequent experiments.[17,18]

Using the database of IS/FS pairs from the SSW sampling determined above, we can identify all the homogeneous transition pathways (see Methodology section and Fig. 2c). The automated SSW pathway sampling method significantly facilitates the unbiased pathway identification without requiring any *a priori*

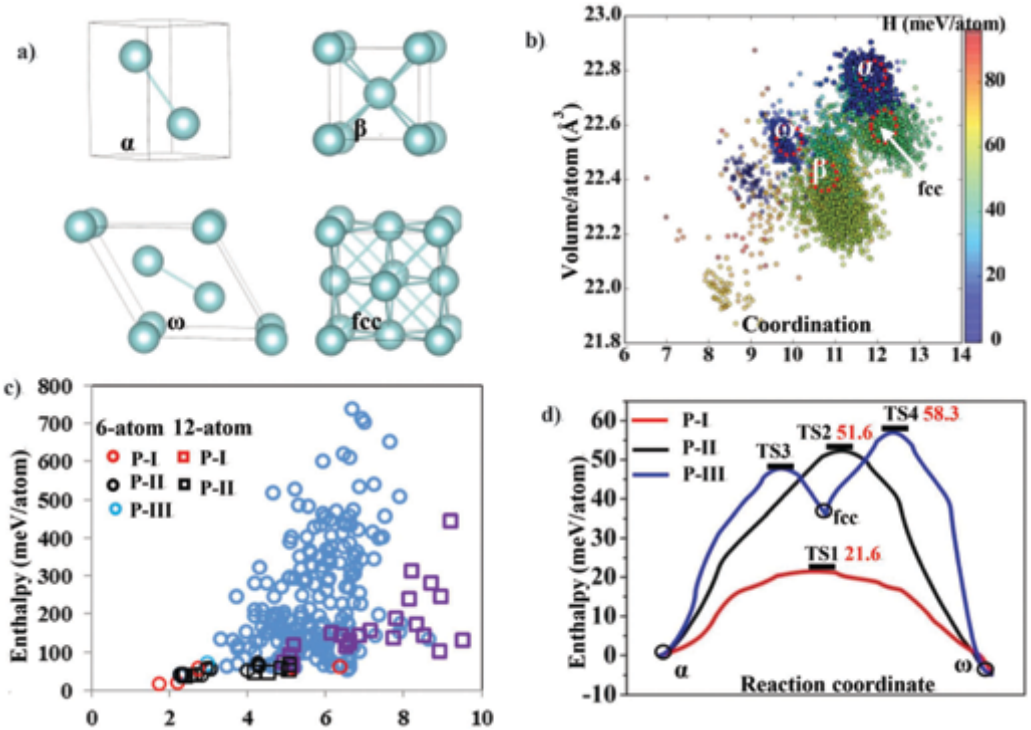

Fig. 2 (a) The common crystal structures of zirconium, including three common phases: α, β, ω phases and a fcc phase (no. 225). Zr atom: cyan. (b) The PES exploration of Zr phases obtained from SSW pathway sampling at 3 GPa. The coordination (x-axis) is calculated using eqn (1). (c) Pathway screening by plotting the approximate energy barrier (eV/6-atom with respect to α phase) *versus* the scaled Euclidean distance (Å) between two phases (measured from the pathways) under 3 GPa. In total, there are 233 pathways from 6-atom sampling and 37 pathways from 12-atom sampling. The approximate barrier is obtained according to DESW pseudopathway, where the maximum energy point along the pathway is generally a good estimate for the true TS.[34] Only the lowest energy pathways, P-I to P-III, are highlighted. (d) Potential energy profile for lowest energy pathways for α–ω solid phase transition at 3 GPa.

knowledge on system (*e.g.* reaction coordinate).[45] Each homogeneous pathway dictates a unique atom displacement pattern, from which the atoms in the IS phase transit to those in the FS phase. Considering that the homogeneous pathways are not real due to the reaction intermediates, the absolute barrier height of these pathways can only be considered as qualitative guidance instead of a kinetic measure. In this work, we have examined a number of distinct low-energy pathways, and all these pathways are further considered as the candidates for the anisotropic phase transition channels. The purpose of the exhaustive homogeneous pathway sampling is, therefore, to identify the possible atom displacement patterns in the phase transition.

From all the homogeneous pathways, we have found the three lowest energy pathways at 3 GPa, namely P-I, P-II and P-III. The calculated enthalpy ($H = E + PV$) barrier of P-I is very low, 21.6 meV per atom relative to α phase, while those for P-II and P-III are 51.6 and 58.3 meV per atom, respectively. The overall potential energy profiles of these pathways are shown in Fig. 1d. Both P-I and P-II are direct pathways with distinct OR: the OR of P-I is $(11\bar{2}2)_\alpha//(1\bar{1}00)_\omega$; $[1\bar{1}00]_\alpha//[11\bar{2}0]_\omega$, equivalent to UZ Variant-I OR in literature; that of P-II is $(10\bar{1}0)_\alpha//(1\bar{1}00)_\omega$; $[0001]_\alpha//[11\bar{2}0]_\omega$, equivalent to UZ Variant-II OR. These are consistent with previous calculations.[29,30] P-III is an indirect channel *via* the fcc phase with an apparent OR $(0001)_\alpha//(02\bar{2}1)_\omega$; $[11\bar{2}0]_\alpha//[2\bar{1}\bar{1}0]_\omega$, which has not been reported. We note that the α–ω phase transition is unlikely to pass β phase: the lowest-energy pathway involving β phase ranks 5th from the lowest to the highest barrier, being energetically very unfavorable compared to others (see ESI†).

The atom displacement patterns of P-I and P-II are highlighted in Fig. 3a, where the variation in the crystallographic planes $(11\bar{2}2)_\alpha//(1\bar{1}00)_\omega$ of P-I and $(10\bar{1}0)_\alpha//(1\bar{1}00)_\omega$ of P-II are focused. In P-I, all atoms displace cooperatively and uniformly, parallel with the $(11\bar{2}2)_\alpha$ plane but towards different directions. The characteristic parallelogram in $(11\bar{2}2)_\alpha$ changes to the rectangular $(1\bar{1}00)_\omega$, resulting in 9.6% shrinking at the $[1\bar{1}00]_\alpha$ direction. By contrast, in P-II, two layer Zr atoms in $(10\bar{1}0)_\alpha$ shuffle oppositely along the $[\bar{1}2\bar{1}0]$ direction. This shear movement does not develop large strains.

The differences of the two phase transition pathways are also evident from the phonon spectra of TSs shown in Fig. 3b–e, where the corresponding atom displacement eigenvectors (red arrows) at the largest imaginary frequency are shown in Fig. 3c and e. The imaginary mode for TS1 of P-I is largely localized at Γ point (low coupling between lattice and atom) with uniform but small-magnitude atom displacement, which exhibits characteristics of the restructuring phase transition.[45] By contrast, the imaginary mode for TS2 of P-II is delocalized across the whole Brillouin zone, featuring a large- magnitude shearing movement of two of every six atom layers in $(10\bar{1}0)_\alpha$ planes. The delocalization of imaginary phonon reflects a strong coupling between lattice and atom displacement, indicating a displacive Martensitic phase transition mechanism.[45]

The homogenous phase transition pathways in Fig. 3 capture the lattice and atom correspondences allowed in the solid phase transition and may also account for the early nucleation of new phases (*e.g.* nearby defects or under very high pressures). However, as for the new phase growth, the anisotropic kinetics turns out to be critical, which requires knowledge on the lowest energy pathways from α to ω mediated by intermediates involving α/ω mixed phases, *i.e.* α → α/ω → ω pathways. In the following, we show that these intermediates can be considered α/ω heterophase junctions, which can be obtained from numerical analysis by assessing the interfacial strain and atom displacement magnitude.

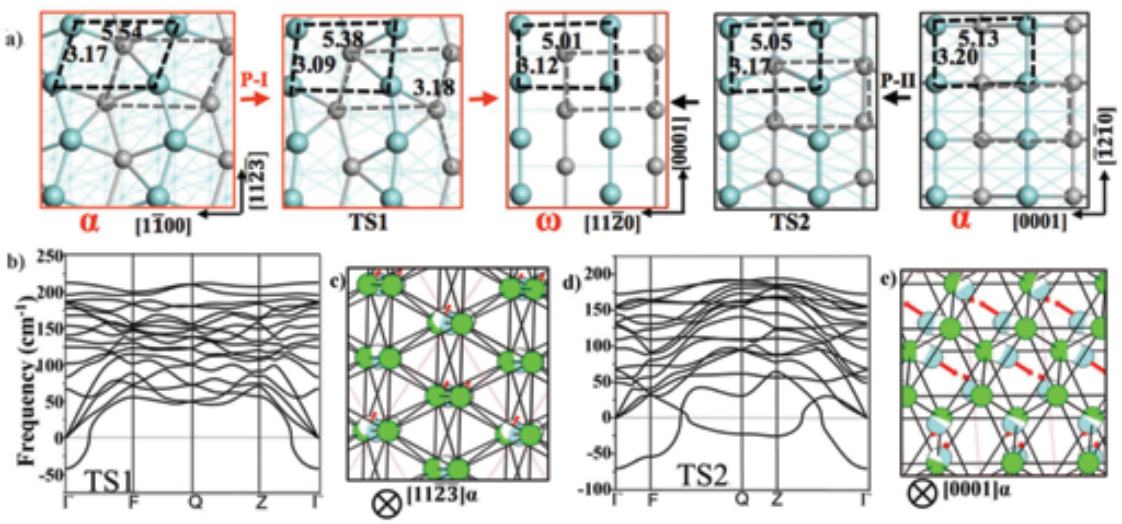

Fig. 3 (a) Snapshots highlighting atom displacement in P-I and P-II pathways viewed down from the determined atomic habit plane, $(11\bar{2}2)_\alpha$ (P-I) and $(10\bar{1}0)_\alpha$ (P-II). The distances indicated are in Å. Cyan and grey: Zr at two different layers. (b–e) Calculated phonon dispersion for TS1 (b) and TS2 (d), and the associated imaginary phonon displacement eigenvectors (c and e) as represented by red arrows. In (c and e), the original α and ω phases are fitted into the TS lattice (black lines), where green, white and blue balls represent the atoms at α, TS and ω states, respectively. The high-symmetry points of the Brillouin zone are denoted as *Γ* (0, 0, 0); *F* (0, 0.5, 0); *Q* (0, 0.5, 0.5); and *Z* (0, 0, 0.5).

b. Heterophase junctions and pathways. Based on the homogeneous pathways, we can then determine the most stable intermediates in α–ω phase transitions, where the heterophase interfaces are present. The key technique utilized here is a numerical search for atomic habit planes (coherent interface) of α–ω phase transition using the information on atom displacement patterns of the pathway, including the lattice correspondence, atom displacement direction and distances. Our procedure to identify the atomic habit plane for α–ω phase transition is detailed in ESI.† From our studies, we recognized that to generate stable α/ω interfaces, two criterions are critical, namely (i) minimum strain at the interface; and (ii) minimum atom movement perpendicular to the interface planes during phase transformation.

The atomic model for the likely α/ω HJs can then be constructed using the superlattice approach.[46] This can be done by joining two phases in one lattice, *e.g.* with 24 atoms for each side in this work. The three most stable α/ω HJs are screened out from a number of candidates differing by the interface, as listed in Table 1. Their structures are shown in Fig. 4 and also in ESI.† No stable HJ intermediates related to P-III are found due to the too-large strain of α/ω interface. We found that the HJ with the lowest interfacial energy in different ORs are the HJ-I, $(11\bar{2}2)_\alpha//(1\bar{1}00)_\omega$ from P-I, and HJ-II, $(10\bar{1}0)_\alpha//(1\bar{1}00)_\omega$ from P-II, as shown in Fig. 4. These two interfaces are exactly the crystallographic planes with the minimum atom perpendicular movement in phase transition.

The $(10\bar{1}0)_\alpha//(1\bar{1}00)_\omega$ of HJ-II has a low strain at the interface (within 2.3%), while the $(11\bar{2}2)_\alpha//(1\bar{1}00)_\omega$ of HJ-I has a much larger strain (9.6%) at the $[1\bar{1}00]_\alpha$ direction. Consequently, their interfacial energies are computed as 4 and 20 meV Å^{-2}, respectively, from DFT. These results show that, interestingly, the HJ intermediate from the lowest homogeneous barrier pathway (P-I, OR-I) is in fact much less stable compared to that from the higher-barrier pathway (P-II, OR-II). This provides direct evidence that the homogeneous phase transition model cannot predict the stability of the phase propagation intermediates.

In the final step, the energy profiles of heterogeneous phase transition pathways are calculated.

With the known structure of the intermediates, the α/ω HJ in superlattice, and the associated atom displacement pattern, the procedure to determine the energy profile is similar to that in the homogeneous pathway using the DESW method, except a large superlattice is utilized as the unit cell. The energy profiles of the three lowest energy pathways mediated by three α/ω HJs, namely, P(HJ-*x*, *x* = I, II, III), are shown in Fig. 4, and the data are listed in Table 1.

Table 1 Energetics of heterogeneous pathways and heterophase junctions for α–ω phase transition of Zr at 3 GPa. γ (meV Å^{-2}) is the interfacial energy[46] and H_a is the heterogeneous transition barrier (meV per interface atom)

HJ	Interface	OR	γ	H_a
I	$(11\bar{2})\alpha//(1\bar{1}00)_\omega$	OR-I	20	185
II	$(10\bar{1}0)\alpha//(1\bar{1}00)_\omega$	OR-II	4	168
III	$(0001)\alpha//(11\bar{2}0)_\omega$	OR-II	8	257
IV	$(1\bar{1}01)\alpha//(01\bar{1}1)_\omega$	OR-II	33	—
V	$(\bar{1}2\bar{1}1)\alpha//(1\bar{1}00)_\omega$	OR-I	Unstable	—
VI	$(0001)\alpha//(01\bar{1}1)_\omega$	OR-I	Unstable	—

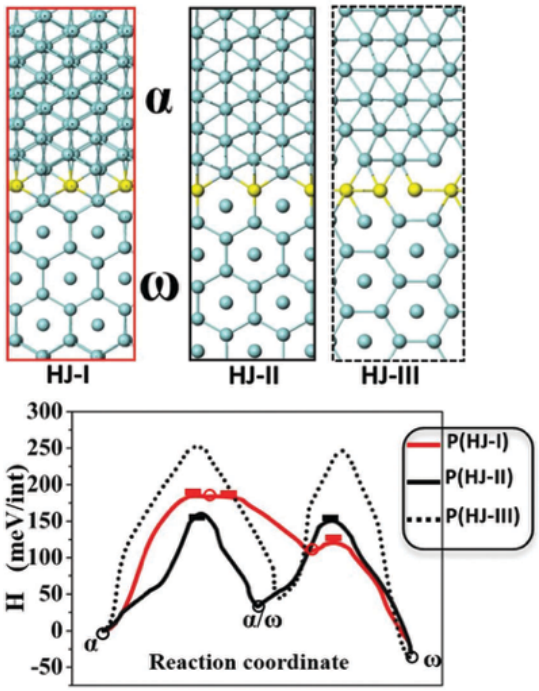

Fig. 4 Top: Three most stable α/ω HJs obtained from P-I and II pathways. HJ-I: $(11\bar{2}2)_\alpha//(1\bar{1}00)_\omega$; HJ-II: $(10\bar{1}0)_\alpha//(1\bar{1}00)_\omega$; HJ-III: $(0001)_\alpha//(11\bar{2}0)_\omega$. Bottom: Potential energy profile of lowest energy heterogeneous transition pathways, (α → α/ω → ω) *via* three different HJs.

By focusing on the two lowest energy heterogeneous pathways, P(HJ-I) and P(HJ-II), and varying the external pressure (hydrostatic), we further evaluated the pressure dependence of the anisotropic phase propagation kinetics. The effective barrier of the two pathways (the highest barrier in α → α/ω → ω, see Fig. 4) at different pressures are plotted in Fig. 5 (solid lines) together with the relative stability ($\Delta H_{\alpha/\omega}$) of the α/ω HJ intermediate (dotted lines). In general, the barrier decreases with the increase of pressure, consistent with the general knowledge on the pressure-induced α → ω transformation. Importantly, in the pressure range investigated, two likely phase transition pathways with different mechanisms (OR) coexist in one system. From the energy profile, H_a is close to $\Delta H_{\alpha/\omega}$ in the P(HJ-I), but

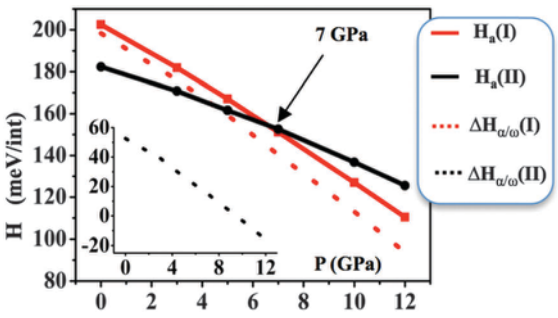

Fig. 5 Pressure dependence of the enthalpy barrier (H_a) and the relative stability ($\Delta H_{\alpha/\omega}$) of the α/ω HJ intermediates (both with respect to α phase in meV per interface atom) in two heterogeneous pathways *via* HJ-I and HJ-II. $\Delta H_{\alpha/\omega}$(II), being much lower than others, is shown separately in inset.

$\Delta H_{\alpha/\omega}$ is much lower than H_a in the P(HJ-II). The barrier of P(HJ-I) is thus mainly caused by the unstable HJ-I interface, but this is not true for P(HJ-II).

Fig. 5 shows that P(HJ-II) with OR-II is preferred at relatively low pressures for both thermodynamics (stable interface intermediate) and kinetics (lower barrier of phase growth). This supports OR-II under equilibrium experiment conditions that can be observed using time-resolved techniques such as *in situ* X-ray diffraction.[23] On the other hand, P(HJ-I) with OR-I is only likely at high-pressure conditions. The stability of its HJ is the bottleneck in the phase propagation. Experimentally, the high static pressure or shock-loaded experiments tend to yield OR-I between coexisting phases.[16,19,28] The phase transformation at these conditions can lead to fast nucleation with the homogenous pathway P-I and short-time growth with the heterogeneous pathway *via* HJ-I. The applied pressure can therefore change the mechanism and OR of the α–ω phase transition.

The puzzle of the reversibility of the α–ω transformation is also closely related to the presence of two distinct reaction channels in the phase transition. From our results, P(HJ-II) that occurs at low pressure is a reversible channel, where the low strain, stable heterophase junction is present as the key structural unit to memorize the reaction pathway, a shape memory effect. The recent experiment by Wenk *et al.*[23] confirms that the α–ω phase transition is perfectly reversible at low pressures (1.5–4.5 GPa) with OR-II. P(HJ-I), by contrast, develops a large strain at the phase boundaries, the release of which inevitably creates structural dislocations and defects during phase transformation. The phase transition is thus irreversible, as supported by the high density of dislocation defects observed under high-pressure experiment,[28] where OR-I is determined for the phase transition.

We emphasize that the structure of HJ is critical to the mechanical properties of the material. The HJ-II that appears at low pressures exhibits a large increase in mechanic brittleness, where the theoretical brittleness from bulk and shear modulus (B/G) is only 2.02 (*c.f.* 2.69 for α phase and 2.06 for ω phase). This suggests a marked change of mechanical strength even at an early stage of phase transition after a low fraction of ω phase forms.

5. Conclusion

By developing a general theory of heterogeneous solid phase transition, we here resolve the mechanism of α–ω metal phase transition that has been disputed for over 50 years. We identify two major types of HJs with distinct OR in α–ω phase transition, each being responsible for one heterogeneous phase transition channel. Importantly, the α–ω phase transition can follow both reconstructive and displacive Martensitic phase transition pathways during phase propagation, despite the homogeneous barrier of the reconstructive pathway being significantly lower. The displacive Martensitic pathway, as dominated by shear movement, turns out to have a lower barrier in phase growth due to the energetically favored heterophase junction. The heterogeneity in transition is thus found to be critical in transition kinetics, which is the key to settling the long debate on the α–ω transition mechanism. The new methodology for predicting anisotropic kinetics of solid phase transition provides a quantitative framework for the design of materials *via* controlled solid phase transition.

Acknowledgements

This work is supported by the National Science Foundation of China (21173051, 21361130019, and 21533001), 973 program (2011CB808500, 2013CB834603), Science and Technology Commission of Shanghai Municipality (08DZ2270500), and Program for Professor of Special Appointment (Eastern Scholar) at Shanghai Institute of Higher Learning.

References

1 N. N. Thadhanit; and M. A. Meyers, *Prog. Mater. Sci.*, 1986, **30**, 1–37.
2 S. E. Offerman, N. H. v. Dijk, J. Sietsma, S. Grigull, E. M. Lauridsen, L. Margulies, H. F. Poulsen, M. T. Rekveldt and S. v. d. Zwaag, *Science*, 2002, **298**, 1003–1005.
3 J. S. Bowles and J. K. Machenzie, *Acta Metall.*, 1954, **2**, 129–138.
4 L. D. Laudau and E. M. Lifshitz, *Statistical Physics*, Pergamon Press, Oxford, 1958.
5 S. K. Sikka, Y. K. Vohra and R. Chidambaram, *Prog. Mater. Sci.*, 1982, **27**, 245–310.
6 M. Geetha, A. K. Singh, R. Asokamani and A. K. Gogia, *Prog. Mater. Sci.*, 2009, **54**, 397–425.
7 R. W. Schutz and H. B. Watkins, *Mater. Sci. Eng., A*, 1998, **243**, 305–315.
8 J. C. Williams and E. A. Starke, *Acta Mater.*, 2003, **51**, 5775–5799.
9 Y.-J. Hao, L. Zhang, X.-R. Chen, L.-C. Cai, Q. Wu and D. Alfè, *Phys. Rev. B: Condens. Matter Mater. Phys.*, 2008, **78**, 134101.
10 H. Xia, S. J. Duclos, A. L. Ruoff and Y. K. Vohra, *Phys. Rev. Lett.*, 1990, **64**, 204–207.
11 Y. Zhao, J. Zhang, C. Pantea, J. Qian, L. L. Daemen, P. A. Rigg, R. S. Hixson, G. T. Gray, Y. Yang, L. Wang, Y. Wang and T. Uchida, *Phys. Rev. B: Condens. Matter Mater. Phys.*, 2005, **71**, 184119.
12 J. C. Jamieson, *Science*, 1963, **140**, 72–73.
13 B. S. Hickman, *J. Mater. Sci.*, 1969, 554–563.
14 H. Dammak, A. Dunlop and D. Lesueur, *Philos. Mag. A*, 1999, **79**, 147–166.
15 W. Liu, B. Li, L. Wang, J. Zhang and Y. Zhao, *Phys. Rev. B: Condens. Matter Mater. Phys.*, 2007, **76**, 144107.
16 M. P. Usikov and V. A. Zilbershtein, *Phys. Status Solidi A*, 1973, **19**, 53–58.
17 A. Rabinkin, M. Talianker and O. Botstein, *Acta Metall.*, 1980, **29**, 691–698.
18 S. G. Song and G. T. Gray, *Philos. Mag. A*, 1995, **71**, 275–290.
19 G. Jyoti, K. D. Joshi, S. C. Gupta and S. K. Sikka, *Philos. Mag. Lett.*, 1997, **75**, 291–300.
20 G. Jyoti, R. Tewari, K. D. Joshi, D. Srivastava, G. K. Dey, S. C. Gupta, S. K. Sikka and S. Banerjee, *Defect Diffus. Forum*, 2008, **279**, 133–138.

21 H. Zong, T. Lookman, X. Ding, C. Nisoli, D. Brown, S. R. Niezgoda and S. Jun, *Acta Mater.*, 2014, **77**, 191–199.
22 A. R. Kutsar, I. V. Lyasotski, A. M. Podurets and A. F. Sanches-bolinches, *High Pressure Res.*, 1990, **4**, 475–477.
23 H. R. Wenk, P. Kaercher, W. Kanitpanyacharoen, E. Zepeda-Alarcon and Y. Wang, *Phys. Rev. Lett.*, 2013, **111**, 195701.
24 J. M. Silcock, *Acta Metall.*, 1958, **6**, 481–493.
25 H. Zong, T. Lookman, X. Ding, S.-N. Luo and J. Sun, *Acta Mater.*, 2014, **65**, 10–18.
26 E. Cerreta, G. T. Gray, R. S. Hixson, P. A. Rigg and D. W. Brown, *Acta Mater.*, 2005, **53**, 1751–1758.
27 A. K. Singh, M. Mohan and C. Divakar, *J. Appl. Phys.*, 1983, **54**, 5721–5726.
28 S. Song and G. T. Gray, *AIP Conf. Proc.*, 1994, **309**, 251–254.
29 P. S. Ghosh, A. Arya, R. Tewari and G. K. Dey, *J. Alloys Compd.*, 2014, **586**, 693–698.
30 D. R. Trinkle, R. G. Hennig, S. G. Srinivasan, D. M. Hatch, M. D. Jones, H. T. Stokes, R. C. Albers and J. W. Wilkins, *Phys. Rev. Lett.*, 2003, **91**, 025701.
31 C. Shang and Z. P. Liu, *J. Chem. Theory Comput.*, 2013, **9**, 1838–1845.
32 X. J. Zhang, C. Shang and Z. P. Liu, *J. Chem. Theory Comput.*, 2013, **9**, 3252–3260.
33 C. Shang, X. J. Zhang and Z. P. Liu, *Phys. Chem. Chem. Phys.*, 2014, **16**, 17845–17856.
34 X.-J. Zhang, C. Shang and Z.-P. Liu, *J. Chem. Theory Comput.*, 2013, **9**, 5745–5753.
35 C. Shang and Z. P. Liu, *J. Chem. Theory Comput.*, 2012, **8**, 2215–2222.
36 C. Shang and Z.-P. Liu, *J. Chem. Theory Comput.*, 2010, **6**, 1136–1144.
37 X. J. Zhang and Z. P. Liu, *J. Chem. Theory Comput.*, 2015, **11**, 4885–4894.
38 D. Sheppard, P. Xiao, W. Chemelewski, D. D. Johnson and G. Henkelman, *J. Chem. Phys.*, 2012, **136**, 074103.
39 G. Kresse and J. Furthmüller, *Phys. Rev. B: Condens. Matter Mater. Phys.*, 1996, **54**, 11169–11186.
40 G. Kresse and J. Furthmüller, *Comput. Mater. Sci.*, 1996, **6**, 15–50.
41 P. E. Blöchl, *Phys. Rev. B: Condens. Matter Mater. Phys.*, 1994, **50**, 17953–17979.
42 J. P. Perdew, K. Burke and M. Ernzerhof, *Phys. Rev. Lett.*, 1998, **80**, 891.
43 G. Kresse, J. FurthmüLler and J. Hafner, *Europhys. Lett.*, 1995, **32**, 729–734.
44 W. Frank, C. Elsässer and M. Fähnle, *Phys. Rev. Lett.*, 1995, **74**, 1791–1794.
45 S. H. Guan, X. J. Zhang and Z. P. Liu, *J. Am. Chem. Soc.*, 2015, **137**, 8010–8013.
46 W. N. Zhao, S. C. Zhu, Y. F. Li and Z. P. Liu, *Chem. Sci.*, 2015, **6**, 3483–3494.

